Journal of Autoimmunity 105 (2019) 102296

Contents lists available at ScienceDirect

Journal of Autoimmunity

journal homepage: www.elsevier.com/locate/jautimm

PD-1 aborts the activation trajectory of autoreactive CD8$^+$ T cells to prohibit their acquisition of effector functions

Hikari Okamura[a,b], Il-mi Okazaki[a], Kenji Shimizu[a], Takumi Maruhashi[a], Daisuke Sugiura[a], Reina Mizuno[a], Taku Okazaki[a,*]

[a] Division of Immune Regulation, Institute of Advanced Medical Sciences, Tokushima University, Tokushima, 770-8503, Japan
[b] Immunology Research Unit, Department of Medical Innovations, Otsuka Pharmaceutical Co., Ltd., Tokushima, 771-0130, Japan

ARTICLE INFO

Keywords:
PD-1
Type I diabetes
Single cell analysis
Pseudotime ordering

ABSTRACT

Anti-PD-1 therapy can induce eradication of tumors and immune-related adverse events (irAEs) in humans and model animals. However, how *anti*-PD-1 therapy modifies cellular phenotypes of CD8$^+$ T cells to destroy tumors and damage self-tissues remains to be clarified. Here we performed single cell mRNA expression profiling of autoreactive CD8$^+$ T cells under or beyond PD-1 suppression in target tissues and reconstructed their activation trajectory. Autoreactive CD8$^+$ T cells went through four activation phases and PD-1 strongly attenuated the transition from the second- to the third-phase, where effector functions were acquired. Shifts in cluster composition of autoreactive CD8$^+$ T cells markedly reflected the severity of autoimmunity. In addition, genes up-regulated along the activation-trajectory in autoimmunity were highly expressed in responders of melanoma patients in *anti*-PD-1 therapy, suggesting that tumor-specific T cells need to be activated in a similar trajectory to destroy tumors in human patients upon PD-1 blockade. These findings reveal that PD-1 blockade facilitates the activation trajectory of CD8$^+$ T cells to boost their effector functions. Targeted manipulation of the trajectory could lead to new therapeutic opportunities.

1. Introduction

Due to the success of *anti*-PD-1 therapy in the treatment of cancer with the occasional development of immune-related adverse-events (irAEs), PD-1 is widely accepted as an immune-checkpoint receptor that serves to restrict immune responses against self-tissues and tumor cells [1–6]. However, it remains unclear how PD-1 modifies cellular phenotypes of T cells specific to self- and tumor-antigens to avoid autoimmunity and hamper tumor-eradication.

Engagement of PD-1 with either PD-L1 or PD-L2 during antigen stimulation results in the phosphorylation of two tyrosine residues in the cytoplasmic region of PD-1, the recruitment of protein tyrosine phosphatase, SHP-2 to the distal phospho-tyrosine, and the decreased phosphorylation of various signaling molecules. Thereby, PD-1 inhibits T cell receptor (TCR)-dependent activation of T cells to suppress their proliferation, cytokine production, and cytotoxicity [7–11]. Besides, PD-1 has been reported to induce anergy and exhaustion of T cells or instruct the differentiation of regulatory T cells [12–15]. Therefore, *anti*-PD-1 therapy is presumed to activate T cells by abrogating these PD-1 functions in the eradication of tumors as well as destruction of self-tissues.

Actually, PD-1 blockade has been shown to increase the number of antigen specific CD8$^+$ T cells in mouse models of chronic viral infection [14–17]. These CD8$^+$ T cells showed higher capacity to produce cytokines such as IFNγ and TNF upon *ex vivo* re-stimulation with antigen. However, the expression of effector molecules without *ex vivo* re-stimulation was marginal or transient, and thus how and where these CD8$^+$ T cells acquire curative effector function upon PD-1 blockade remains to be elucidated. In the *anti*-PD-1 cancer immunotherapy, signatures of T cells such as activation, exhaustion, cytotoxicity, IFNγ response, and proliferation in tumor tissues have been shown to correlate with the outcome of the therapy [18–21]. However, the magnitude of up-regulation of individual genes upon *anti*-PD-1 therapy was limited or unspecified, making the actual activation status of T cells unintelligible. Riaz et al. estimated the number of each cell type in tumor tissues based on the gene expression profile by using an elaborated deconvolution method and demonstrated a positive correlation between the numbers of CD8$^+$ T and NK cells to the outcome of *anti*-PD-1 therapy [21]. Huang et al. detected the proliferation of T cells in the peripheral blood upon *anti*-PD-1 therapy. Intriguingly, the proliferation of CD8$^+$ T cells

* Corresponding author. Division of Immune Regulation, Institute of Advanced Medical Sciences, Tokushima University, 3-18-15 Kuramoto, Tokushima, 770-8503, Japan.
E-mail address: tokazaki@genome.tokushima-u.ac.jp (T. Okazaki).

https://doi.org/10.1016/j.jaut.2019.06.007
Received 7 May 2019; Received in revised form 19 June 2019; Accepted 19 June 2019
Available online 02 July 2019

in relation to tumor burden showed a positive correlation to the outcome of *anti*-PD-1 therapy, although the expression levels of Perforin and Granzymes in these proliferating $CD8^+$ T cells were rather decreased upon *anti*-PD-1 therapy [22].

Single cell analyses using mass cytometry and RNA sequencing are useful to estimate the states of individual cells and elucidate the cellular mechanisms of various biological phenomena. However, the activation of $CD8^+$ T cells upon PD-1 blockade in tumor tissues or peripheral blood was not evident even with single cell analyses. The increase of $CD8^+$ T cells with the exhausted signature or the lowest Granzyme B expression among tumor-infiltrating lymphocytes has been reported as the hallmark of *anti*-PD-1 therapy in single cell analyses using mass cytometry, which is rather paradoxical to its curative effects [23,24]. By using single cell RNA sequencing, the frequency of memory/effector-like $CD8^+$ T cells in melanoma tissues was found to correlate with the outcome of *anti*-PD-1 therapy [25]. However, the difference likely represents the difference in tumors and microenvironments rather than the differential response to *anti*-PD-1 therapy among patients because the difference was not observed between samples before and after *anti*-PD-1 therapy [25]. Thus, the activation of $CD8^+$ T cells upon *anti*-PD-1 blockade has not been evident in former single cell analyses contrary to the general expectations, making the cellular mechanisms of tumor-eradication and irAEs by *anti*-PD-1 therapy remain unclear.

In the current study, we performed a quantitative PCR-based single cell expression profiling and pseudotemporal analyses to explore the trajectory of autoreactive $CD8^+$ T cells that are responsible for the fulminant type I diabetes (T1D) in NOD mice upon PD-1 blockade. First, we identified the trajectory of autoreactive $CD8^+$ T cells with four distinct states. Next we found that autoreactive $CD8^+$ T cells went through four activation phases. Remarkably, PD-1 strongly attenuated the transition from the second- to the third-phase, where effector functions were acquired. We further demonstrated that shifts in cluster composition markedly reflected severity of T1D in mouse. Finally, we analyzed the gene expression in melanomas of human patients. Genes representing functionally enabled T cells upon PD-1 blockade in T1D showed higher expression in melanoma tissues of responders after *anti*-PD-1 therapy. Furthermore, genes representing active suppression by PD-1 in T1D showed higher expression in melanoma tissues of responders before *anti*-PD-1 therapy. These results suggest that tumor-specific T cells are activated in a similar trajectory as in T1D to destroy tumors in responders upon PD-1 blockade.

2. Materials and methods

2.1. Mice

NOD/ShiJcl mice were purchased from Japan CLEA and housed under specific pathogen-free conditions in environmentally controlled clean rooms. All mouse protocols were approved by the Animal Experimentation Committee of Tokushima University.

2.2. Induction of T1D

Pre-diabetic female NOD mice (10–12 wks-old) were administrated intraperitoneally every other day with *anti*-PD-L1 Ab (1–111A, 500 μg) [26]. Mice were considered diabetic after two consecutive blood glucose measurements exceeded 250 mg/dL. Rat IgG2a (RTK2758, BioXCell) was used for control. $CD4^+$ and $CD8^+$ T cells were depleted by the intravenous injection of Abs against CD4 (GK1.5, 200 μg) and CD8 (53–6.7, 200 μg) on days −3, 1, and 5.

2.3. Isolation of islet-infiltrating lymphocytes

Islet infiltrates were prepared from pre-diabetic NOD mice treated with or without *anti*-PD-L1 Ab as previously described [27]. Briefly, pancreata were dispersed into single cell suspensions by collagenase (Wako) and DNase I (Sigma-Aldrich). Islet-infiltrating lymphocytes were enriched by Percoll gradient centrifugation (GE Healthcare).

2.4. Detection of proliferating cells in mice

Pre-diabetic NOD mice were treated with or without *anti*-PD-L1 Ab on days 0 and 2 and EdU (5-ethynyl-2'-deoxyuridine, 1 mg, Sigma-Aldrich) on day 2. Pancreatic infiltrates, pancreatic LN cells, and spleen cells were prepared on day 4. Ghost Dye Violet 510 (TNBO, 13–0870) was used to distinguish live from dead cells. EdU-incorporated cells were detected using Click-iT Plus Alexa Fluor 647 Picolyl Azide Toolkit (Invitrogen) according to the manufacturer's instructions.

2.5. Flowcytometric analysis

Splenocytes, islet-infiltrating lymphocytes, and pancreatic LN cells were stained with indicated antibodies. Data were obtained with Gallios (Beckman Coulter) and analyzed using FlowJo (Tree Star) or Cytobank (Cytobank). Fluorochrome-conjugated Abs against mouse CD3e (145-2C11), mouse TCRβ (H57-597), mouse CD8α (53–6.7), mouse CD4 (GK1.5 and RM4-5), mouse/human CD44 (IM7), mouse CD45 (30-F11), mouse CD62L (MEL-14), mouse CD69 (H1.2F3), human/mouse/rat ICOS (C398.4A), mouse CD366 Tim-3 (RMT3-23), and mouse PD-1 (RMP1-30), biotinylated Abs against mouse/human CD11b (M1/70), mouse CD11c (N418), mouse CD45R/B220 (RA3-6B2), mouse Gr1 (RB6-8C5), mouse Ter-119 (TER-119), and mouse PD-1 (RMP1-30) mAb, and Brilliant Violet 421 (BV421)-conjugated streptavidin were purchased from Biolegend. PE-conjugated streptavidin was purchased from BD Pharmingen. Propidium Iodide was used to distinguish live from dead cells.

2.6. Single cell expression profiling

Islet-infiltrating lymphocytes were stained with biotinylated Abs against CD11b, CD11c, CD45R/B220, Gr1, and Ter-119 together with fluorochrome-conjugated Abs against CD8α, CD4, and PD-1. Biotinylated Abs were detected with streptavidin-BV421. $PD\text{-}1^+CD8^+$ T cells were sorted from islet-infiltrating lymphocytes using MoFlo XDP (Beckman Coulter). Single cells of sorted $PD\text{-}1^+CD8^+$ T cells were captured and lysed on chip using the C_1 Single-Cell Auto Prep System (Fluidigm). Reverse transcription and pre-amplification of cDNA library were performed on chip according to the manufacturer's instructions using a pool of 139 primer pairs specific to genes that are known to function in immune cells. Single cell real-time quantitative PCR analyses were performed using nested primer pairs and 2x SsoFast EvaGreen Supermix with Low ROX (BioRad) in 96.96 Dynamic Array IFCs on the BioMark HD system (Fluidigm) according to the manufacturer's instructions. Based on Ct values calculated by the Biomark software, expression levels of genes in each single cell were calculated (Supplemental dataset 1). Out of 178 cells, 3 cells with *Gapdh* expression values falling outside the 95% confidence interval were excluded from subsequent analyses. ANOVA was performed using the SINGuLAR Analysis Toolset v3.5.2 (Fluidigm). Heat maps, violin plots, and volcano plots were generated using the ggplot2 R package. PCA was performed using the ade4 R package. To cluster single cells, k-means^{++} clustering was performed using the LICORS R package.

2.7. Pseudotemporal ordering

The Monocle 2 package was used to analyse trajectories of cells in order to discover activation transitions. 'DDRTree' was applied to reduce dimensions and the visualization functions 'plot_cell_trajectory' or 'plot_complex_cell_trajectory' were used to plot the minimum spanning tree on cells.

2.8. Dimentionality reduction

Visual stochastic neighbour embedding (viSNE) analysis was performed on cytometry data using Cytobank (Cytobank).

2.9. Quantitative PCR

Total RNA was extracted from the single cell suspension of pancreas using TRIzol (Ambion) and subjected to reverse transcription using High-Capacity cDNA Reverse Transcription Kit (Applied Biosystems). Gene expression was analyzed by quantitative PCR using Power SYBR Green PCR Master mix (Applied Biosystems) on a 7900HT Fast Real-time PCR (Applied Biosystems). Values were normalized to the expression of *Gapdh*. Specific primer sets are listed in Supplemental Table 1.

2.10. Gene expression in human melanoma samples

Normalized fragments per kilobase per million mapped reads (FPKM) of genes in human melanoma samples before or after the *anti*-PD-1 therapy with Nivolumab were obtained from Gene Expression Omnibus dataset (GSE91061). We examined the expression levels of genes that showed higher expression in C1–2 cells compared with C3–4 cells in human melanoma samples after the *anti*-PD-1 therapy. We also examined the expression levels of genes that showed higher expression in C3–4 cells compared with C6 cells in human melanoma samples before the *anti*-PD-1 therapy. Patients were divided into responders (complete response, CR or partial response, PR), stable disease (SD), and non-responders (progressive disease, PD) according to the curative effects of *anti*-PD-1 therapy. Expression levels of genes were compared among three groups. Box plots were generated using the ggplot2 R package.

2.11. Statistics

Two-tailed paired Student's t-test was used to evaluate statistical significance unless otherwise indicated. $p < 0.05$ was considered statistically significant.

3. Results

3.1. $CD8^+$ T cells are pathogenic in the fulminant T1D of NOD mice upon PD-1 blockade

PD-1 persistently suppresses the activity of autoreactive T cells in pre-diabetic NOD mice as evidenced by the rapid induction of T1D upon PD-1 blockade with *anti*-PD-L1 Ab and the early onset of T1D in NOD-*Pdcd1*$^{-/-}$ mice (Fig. 1A) [28–30]. $CD8^+$ T cells play the pathogenic role in this rapid manifestation of T1D because the depletion of $CD8^+$ but not $CD4^+$ T cells strongly attenuated the development of T1D upon PD-1 blockade (Fig. 1A). About 30% of islet-infiltrating $CD8^+$ T cells in pre-diabetic NOD mice expressed PD-1, suggesting that these PD-1^+CD8^+ T cells were under the control of PD-1. Upon PD-1 blockade with *anti*-PD-L1 Ab, islet-infiltrating $CD8^+$ T cells were rapidly activated to express PD-1 and start proliferation (Fig. 1B and Supplemental Fig. S1). These $CD8^+$ T cells are beyond the control of PD-1 and likely included autoreactive $CD8^+$ T cells that actively destroyed β cells. Although PD-1-expressing and proliferating $CD8^+$ T cells were markedly increased in islets, their increases were insignificant or marginal in pancreatic LNs and spleen, suggesting that PD-1 mainly functions in target organs rather than in draining LNs in the regulation of autoreactive $CD8^+$ T cells in NOD mice as suggested before (Supplemental Fig. S1) [30–32]. Therefore, we focused on islet-infiltrating PD-1^+CD8^+ T cells in the subsequent analyses.

3.2. Clustering of autoreactive $CD8^+$ T cells under or beyond the control of PD-1

To characterize autoreactive $CD8^+$ T cells under or beyond the control of PD-1, we prepared single PD-1^+CD8^+ T cells from pancreata of pre-diabetic NOD mice with or without PD-1 blockade (PD1posA and PD1posC cells for PD-1 positive cells of Ab-treated and control mice, respectively) (Fig. 1B). Islet-infiltrating PD-1^-CD8^+ T cells from pre-diabetic NOD mice without PD-1 blockade were used as control (PD1negC cells). We evaluated the expression of 139 genes by quantitative PCR in a total of 175 single cells (PD1posA; 82 cells from 2 mice, PD1posC; 49 cells from 12 mice, and PD1negC; 44 cells from 9 mice) and clustered single cells into 6 groups (C1–6 clusters) by using k-means^{++} based on their gene expression profiles (C1; 14 cells, C2; 24 cells, C3; 28 cells, C4; 34 cells, C5; 35 cells, and C6; 40 cells) (Fig. 1C). To explore the molecular identities of single cells, we performed global principal component analysis (PCA) projection of all single cells profiled in this analysis. PD1posA, PD1posC and PD1negC cells were largely separated with substantial overlaps by PCA (Fig. 1D). We could also observe a clear separation of C1–6 cells by PCA (Fig. 1E). Activation-signature genes such as *Cd44*, *Cd38*, and *Icos* showed negative contribution to PC1 (Fig. 1F), suggesting that C1–4 cells represent activated cells and the magnitude of activation likely increase in the order of C4 to C1. Negative contribution of naive-signature genes such as *Sell* (CD62L), *Ccr7*, and *Lef1* to PC2 suggests that C5 cells represent naive cells. On the other hand, C6 cells had high PC1 and PC2 values, suggesting that these cells represent antigen-experienced but inactivated cells that may resemble exhausted T (Tex) cells in chronic viral infection [33].

The composition of clusters largely differed among PD1posA, PD1posC, and PD1negC cells. Naive C5 cells predominated in PD1negC cells, in agreement with the activation-dependent expression of PD-1 (Fig. 1G) [34]. The frequencies of activated C1–C4 cells were largely differed between PD1posA and PD1posC cells (95% vs. 35% for PD1posA and PD1posC cells, respectively). Remarkably, activated PD1posC cells were composed of C3 and C4 cells, whereas PD1posA cells included C1 and C2 cells in addition to C3 and C4 cells, indicating that PD-1 restrains the transition from C3 to C2. More than half of PD1posC cells were clustered in C6, suggesting that these autoreactive $CD8^+$ T cells were inactivated by PD-1 engagement (Fig. 1G).

3.3. Delineation of the activation trajectory of autoreactive $CD8^+$ T cells by pseudotemporal ordering

To explore the continuum of activation states in autoreactive $CD8^+$ T cells, we performed pseudotemporal ordering of the single cells by using Monocle 2 [35]. We could reconstruct a trajectory with two branches and four distinct states (Sa to Sd). We detected 69, 23, 44, and 39 cells on the path to Sa, Sb, Sc, and Sd, respectively (Fig. 2A–D and Supplemental Fig. S2A). C5 and C6 cells were concentrated at Sd and Sc tips of the tree, respectively, indicating that these cells are substantially distant from the other cells in pseudotime (Fig. 2, A, C, and D). As for activated C1–4 cells, C1–3 cells lined up on the path to Sa in this order, while the majority of C4 cells occupied the Sb tip of the tree. PD1posA cells were mainly composed of C1, C2, and C3 cells of Sa and C4 cells of Sb (Supplemental Fig. S2B). On the other hand, the majority of PD1posC and PD1negC cells were C6 cells of Sc and C5 cells of Sd, respectively (Supplemental Fig. S2B). The activation-signature of cells (expression levels of *Cd44*, *Cd69*, *Cxcr3*, *Fasl*, *Gzma*, *Gzmb*, *Il2ra*, and

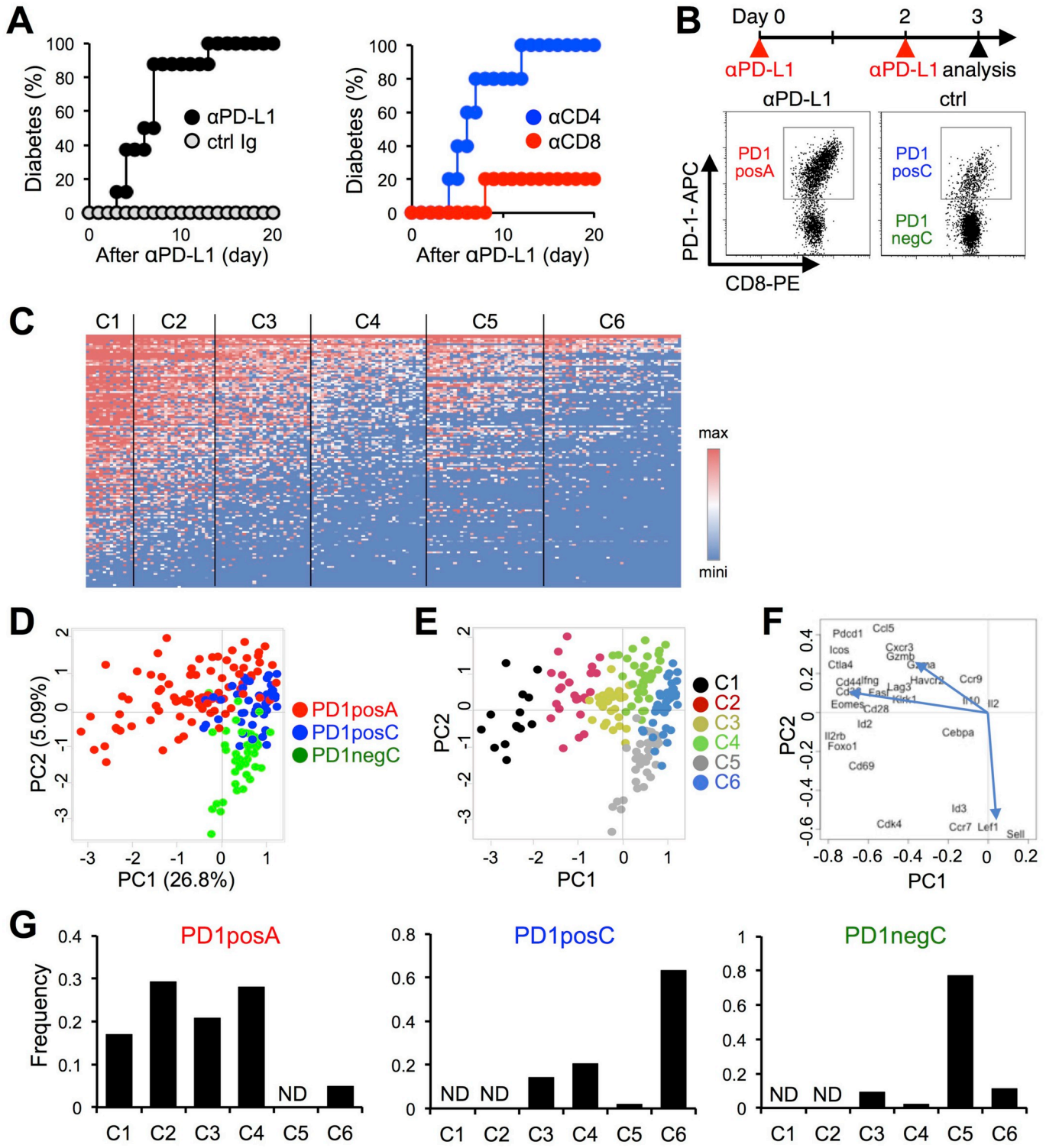

Fig. 1. Clustering of autoreactive CD8$^+$ T cells under and beyond the control of PD-1. (A) Pathogenic role of CD8$^+$ T cells in the rapid manifestation of T1D in pre-diabetic NOD mice upon PD-1 blockade. Diabetic incidence of NOD mice treated with αPD-L1 or its isotype control (ctrl Ig) (n = 8 each) (left). Diabetic incidence of NOD mice depleted of CD4$^+$ (αCD4) or CD8$^+$ (αCD8) T cells upon αPD-L1 treatment (n = 5 each) (right). (B) Preparation of PD-1$^+$CD8$^+$ T cells under or beyond PD-1 control. Schematic representation of the sample preparation (top). PD-1$^+$CD8$^+$ T cells from αPD-L1-treated NOD mice (PD1posA) and PD-1$^+$CD8$^+$ and PD-1$^-$CD8$^+$ T cells from control NOD mice (PD1posC and PD1negC, respectively) were analyzed (bottom). (C) Heat map showing k-means^{++} clustering of PD1posA, PD1posC, and PD1negC cells. A total of 175 single cells were clustered based on the expression of 139 genes. (D–F) PCA of single cells. Source (D) and cluster (E) of each cell are shown by color as indicated. Correlations of genes with the principal component 1 (PC1) and PC2 from the PCA are shown (F). (G) Cluster compositions of PD1posA, PD1posC, and PD1negC cells. ND, not detected. (For interpretation of the references to color in this figure legend, the reader is referred to the Web version of this article.)

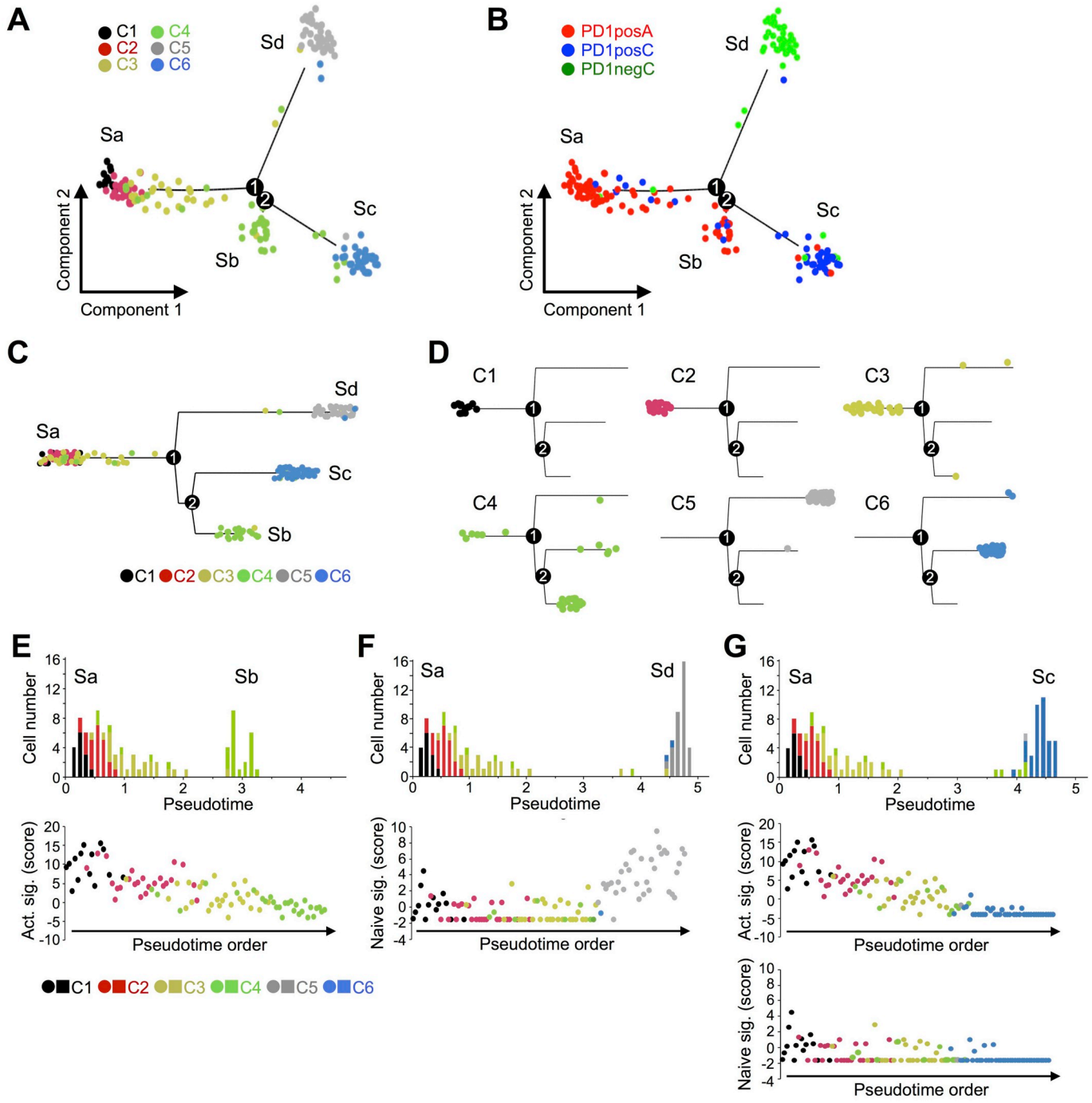

Fig. 2. Activation trajectories of autoreactive CD8$^+$ T cells revealed by the pseudotemporal ordering. (A–D) Pseudotemporal ordering of single cells. Projection into a two-dimensional space (A and B) and tree structure (C and D) by Monocle 2. Four states (Sa to Sd) and two branches (1 and 2) are indicated. Cluster (A) and origin (B) of cells are colored as indicated. Tree structures of C1–6 cells are separately shown (D). (E–G) Changes in naive and activated signatures of cells along with the reconstructed trajectory. Number of cells (top) and naive and activated (Act.) signatures (sig.) of each cell (middle and bottom) plotted with respect to pseudotime and pseudotime order, respectively. Trajectories from Sa to Sb (E), Sa to Sd (F), and Sa to Sc (G) are shown. Cluster of cells are shown by color as indicated. (For interpretation of the references to color in this figure legend, the reader is referred to the Web version of this article.)

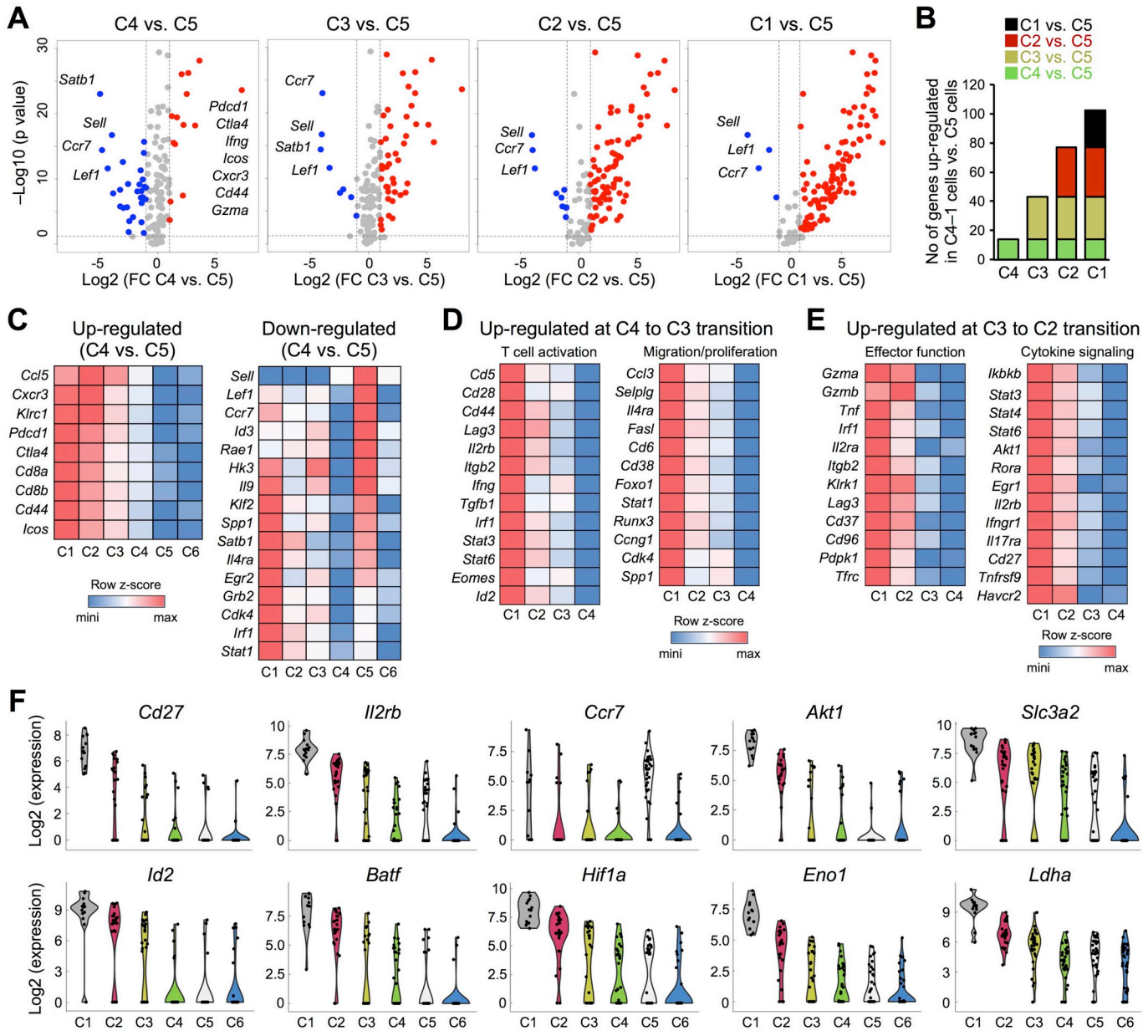

Fig. 3. PD-1 prohibited autoreactive CD8$^+$ T cells from acquiring effector function. (A and B) Sequential up-regulation of genes related to T cell activation in the order of C4 to C1. Volcano plots showing differentially expressed genes between C5 and C4–1 cells (A). Stacked bar graphs indicating the number of genes that were up-regulated in C4–1 cells compared with C5 cells. Genes up-regulated more than 2 folds ($p < 0.05$, ANOVA test) were counted. The number of genes that was additively up-regulated at the indicated comparison is shown with the indicated color (B). (C–E) Heat maps showing the relative expression levels of indicated genes among indicated clusters. Levels of down expression (blue) or up expression (red) are shown on a normalized z-score of each gene among C1–6 (C) and C1–4 cells (D and E). Up-regulated and down-regulated genes in the comparison between C4 and C5 are shown (C). Genes up-regulated in the transition from C4 to C3 (D) and C3 to C2 (E) are shown. (F) Violin plots showing the expression of genes that were highly up-regulated in the transition from C2 to C1. (For interpretation of the references to color in this figure legend, the reader is referred to the Web version of this article.)

Tnf) showed progressive increase along the trajectory from Sb to Sa, suggesting that autoreactive CD8$^+$ T cells were activated sequentially from Sb to Sa (Fig. 2E). In the trajectory from Sa to Sd, the naive-signature of cells (expression levels of *Ccr7*, *Lef1*, and *Sell*) was progressively increased toward Sd, confirming that Sd represents naive state (Fig. 2F). On the other hand, cells near Sc showed low naive- and activation-signatures, indicating that Sc represents inactivated state (Fig. 2G).

3.4. PD-1 interrupts the activation trajectory of autoreactive CD8$^+$ T cells to prohibit their acquisition of effector functions

To further examine the activation trajectory of islet-infiltrating CD8$^+$ T cells, we examined differentially expressed genes among different clusters. As expected, naive-signature genes were highly expressed in C5 cells, confirming that C5 represents migratory naive cells (Fig. 3A). When C1–4 cells were compared individually with C5 cells,

the number of up-regulated genes was additively increased in the order of C4 to C1 (14, 43, 77, and 102 genes in C4, C3, C2, and C1 vs. C5 comparisons, respectively), further supporting the sequential activation of autoreactive $CD8^+$ T cells in this order (Fig. 3A and B, and Supplemental Figs. S3 and S4). The expression levels of *Klf2*, *Ccr7*, *Lef1*, and *Id3* were decreased in C4 compared with C5 but increased in C3 (Fig. 3C and Supplemental Fig. S5). Because these genes have been reported to show a biphasic expression pattern with transient down-regulation in the initial phase of T cell activation [36–40], C4 likely represents primed cells that have immigrated from draining lymph nodes and C3 represents re-activated cells in islets.

At the transition from C4 to C3, we found the up-regulation of a variety of genes including those related to activation (e.g., *Cd5* and *Cd44*), migration (e.g., *Ccl3* and *Selplg*), and proliferation (e.g., *Cd38, Foxo1*, and *Cdk4*) (Fig. 3D and Supplemental Fig. S5). FoxO1 has been reported to hinder the effector differentiation of $CD8^+$ T cells by up-regulating *Pdcd1* [41,42], suggesting that the activation of $CD8^+$ T cells was attenuated by FoxO1–PD-1 axis at C3, which is in agreement with the interruption of the C3 to C2 transition by PD-1 among PD1posC cells as mentioned above (Fig. 1G). Upon transition to C2, more diverse genes including those related to effector function (e.g., *Gzma* and *Gzmb*) and cytokine signaling (e.g., *Stat3* and *Akt1*) were up-regulated, indicating that autoreactive $CD8^+$ T cells acquire effector function at this step and PD-1 particularly prohibits the acquisition of effector function by autoreactive $CD8^+$ T cells (Fig. 3E and Supplemental Fig. S5). C1 cells likely include terminal effector and precursors of memory $CD8^+$ T cells because the expression of genes related to terminal effector and memory T cells such as *Cd27*, *Il2rb*, *Akt1, Id2,* and *Batf* were markedly increased at this step (Fig. 3F and Supplemental Fig. S5) [43–45].

3.5. $PD\text{-}1^+CD8^+$ autoreactive T cells subjected to PD-1 blockade are functionally enabled

None of the genes examined was significantly up-regulated in C6 cells compared with C1–4 cells and only two genes, *Ccl5* and *Klrc1* showed significant up-regulation in C6 cells compared with C5 cells (Fig. 4A). Interestingly, the difference in *Pdcd1* expression between C6 and C5 cells was not statistically significant, although the majority of C6 cells but not C5 cells expressed PD-1 protein on their cell surface. This discrepancy is most likely due to the generation of mRNA prior to protein and the differences in the stabilities of *Pdcd1* mRNA and PD-1 protein. Nonetheless, C6 cells expressed substantial number of genes related to metabolism, proliferation, and signal transduction such as *Idh2*, *Mdh2*, and *Akt2* at comparable levels ($-2 < FC < 2$) with C1–4 and C5 cells, indicating that C6 cells maintain the basal metabolic, proliferative, and signaling capacities (Fig. 4B and Supplemental Fig. S6). Against our initial expectation that C6 cells may represent Tex-like cells, they did not substantially express genes related to exhausted, anergic, and senescent T cells, suggesting that C6 cells are intensively inactivated but are different from Tex cells (Fig. 4C) [33,46,47].

The expression of multiple inhibitory receptors such as PD-1, Tim-3, LAG-3, and BTLA is widely regarded as a hallmark of T cell exhaustion [33]. In the current study, the frequency of cells expressing multiple inhibitory receptors among $PD\text{-}1^+$ cells was increased by PD-1 blockade (Fig. 4D). However, cells with multiple inhibitory receptors were concentrated in C1–2 cells and preferentially expressed multiple cytokines (Fig. 4D–F), indicating that these cells had escaped from the suppression by inhibitory receptors and were activated. Hereafter, we call C1 and C2 cells as T enabled (Ten) cells, because these cells were not exhausted but functionally enabled by PD-1 blockade.

Although C1–2 Ten cells were highly activated by escaping PD-1 suppression, not all C1–2 Ten cells expressed effector molecules. So, we explored genes that were differentially expressed in C1–2 Ten cells with or without *Gzma/Gzmb*-expression (Fig. 4G). Among inhibitory molecules, *Btla* and *Cd160* but not *Lag3*, *Ctla4*, and *Pdcd1* were highly expressed in activated C1–2 Ten cells without *Gzma/Gzmb* expression, suggesting that BTLA and CD160 may play complementary roles in the suppression of autoreactive $CD8^+$ T cells when PD-1 function is blocked. The expression of *Havcr2* (Tim-3) and *Cd244* (2B4) was rather higher in C1–2 Ten cells expressing effector molecules, suggesting that these receptors may function in the ensuing phase. Meanwhile, C1–2 Ten cells without *Gzma/Gzmb* expression likely represent memory-precursors because they highly expressed memory-related genes such as *Eomes*, *Cd27*, *Il2rb*, and *Ccr7* [44].

3.6. Cluster composition of autoreactive $CD8^+$ T cells correlates with disease status of T1D in NOD mice

Then we examined the pathological consequence of the shifts in cluster composition. Because there are substantial interindividual differences in the progression of T1D in NOD mice, we examined the possible correlation between the cluster composition and the severity of insulitis among individual pre-diabetic NOD mice. We clustered islet-infiltrating $PD\text{-}1^+CD8^+$ T cells into five groups by using k-means^{++} based on the flowcytometric data, because $PD\text{-}1^+CD8^+$ T cells were mostly divided into five clusters (i.e., C1 to C4 and C6) in the aforementioned single cell gene expression analyses (Fig. 1). When we visualized these cells by *t*-SNE, five groups of cells were clearly separated (Fig. 5A and B). We designated these five groups as C1–C4- and C6-like clusters based on expression profiles of molecules. The frequencies of C1- and C2-like Ten cells were higher while the frequencies of C4- and C6-like cells were lower in mice treated with *anti*-PD-L1 Ab in consistent with the results of single cell gene expression analyses (Fig. 5C). We evaluated the destruction of β cells and the severity of insulitis by quantifying the expression of genes related to β cells and lymphocytes in the pancreatic cell suspension of the same mouse. The expression levels of *Ins1* and *Gcg* but not *Amy2a* and *Lpl* that represent exocrine cells in pancreata showed negative- and positive-correlations to the frequencies of C1/2-like Ten and C6-like cells, respectively (Fig. 5D). Thus, mice with more C1/2-like Ten cells maintained less β cells. The expression levels of *Cd3e*, *Cd38*, *Ifng*, *Prf1*, *Gzma*, and *Gzmb* showed positive and negative correlations to the frequencies of C1/2-like Ten and C6-like cells, respectively. These results demonstrate that the activation status of $CD8^+$ T cells markedly reflects the destruction of β cells and the severity of insulitis.

3.7. Tumor-specific T cells are activated in a similar trajectory found in T1D to destroy tumor-tissues in human melanoma patients upon anti-PD-1 therapy

Finally, we examined the possible involvement of a similar activation trajectory in tumor-specific T cells of human patients receiving *anti*-PD-1 therapy (Fig. 6A). We hypothesized that tumor-specific T cells are activated in a similar trajectory found in T1D to destroy tumor-tissues. To test this hypothesis, we analyzed the data deposited by Chan and colleagues (GSE91061), in which the expression of genes in tumor-tissues before and after *anti*-PD-1 therapy and the responses of patients were collected [21]. Remarkably, genes representing the signature of C1–2 Ten cells (i.e., genes highly expressed in C1–2 Ten cells compared with C3–4 cells) showed higher expression in melanoma tissues of responders compared with those of non-responders after *anti*-PD-1 therapy (Fig. 6B and C). These results indicate that tumor specific T cells need to be activated upon *anti*-PD-1 therapy in a similar trajectory found in T1D to destroy tumor tissues efficiently.

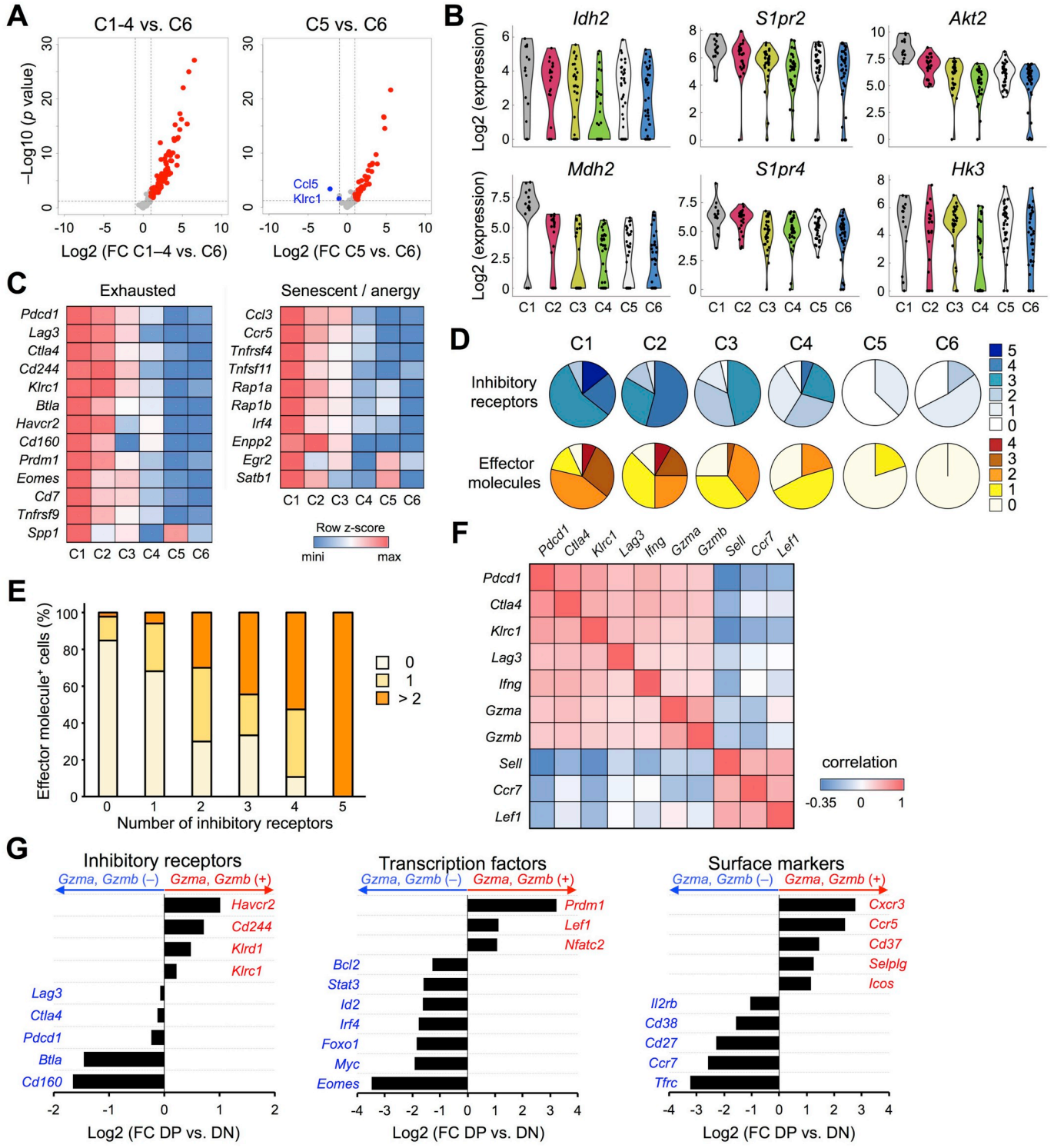

Fig. 4. Preferential expression of effector molecules by cells with multiple inhibitory receptors upon PD-1 blockade. (A) Volcano plots showing differentially expressed genes between C6 and C1–4 or C5 cells. (B) Substantial expression of genes related to metabolism, proliferation, and signal transduction by C6 cells. Violin plots showing the expression of indicated genes in C1–6 cells. (C) No up-regulation of genes related to exhaustion, senescent, and anergy in C6 cells. Heat maps showing the relative expression levels of indicated genes. Levels of down expression (blue) or up expression (red) are shown on a normalized z-score of each gene. (D–F) The expression of multiple inhibitory receptors (*Pdcd1*, *Havcr2*, *Lag3*, *Btla*, and *Klrc1*) and effector molecules (*Gzma*, *Gzmb*, *Ifng*, and *Tnf*) by highly activated T cells upon PD-1 blockade. The frequencies of cells expressing indicated numbers of inhibitory receptors and effector molecules are shown for each cluster (D). The frequencies of cells expressing indicated numbers of effector molecules are shown for cells expressing indicated numbers of inhibitory receptors (E). The correlation coefficients of co-expression were evaluated by nearest-neighbour analysis for indicated gene sets (F). (G) Differentially expressed genes between C1–2 cells with or without effector molecules. Fold-change expression of indicated genes between C1–2 cells double-positive (DP, red) or -negative (DN, blue) for *Gzma* and *Gzmb* are shown in $\log_2$ scale. Genes showed higher expression in DP and DN cells are colored in red and blue, respectively. (For interpretation of the references to color in this figure legend, the reader is referred to the Web version of this article.)

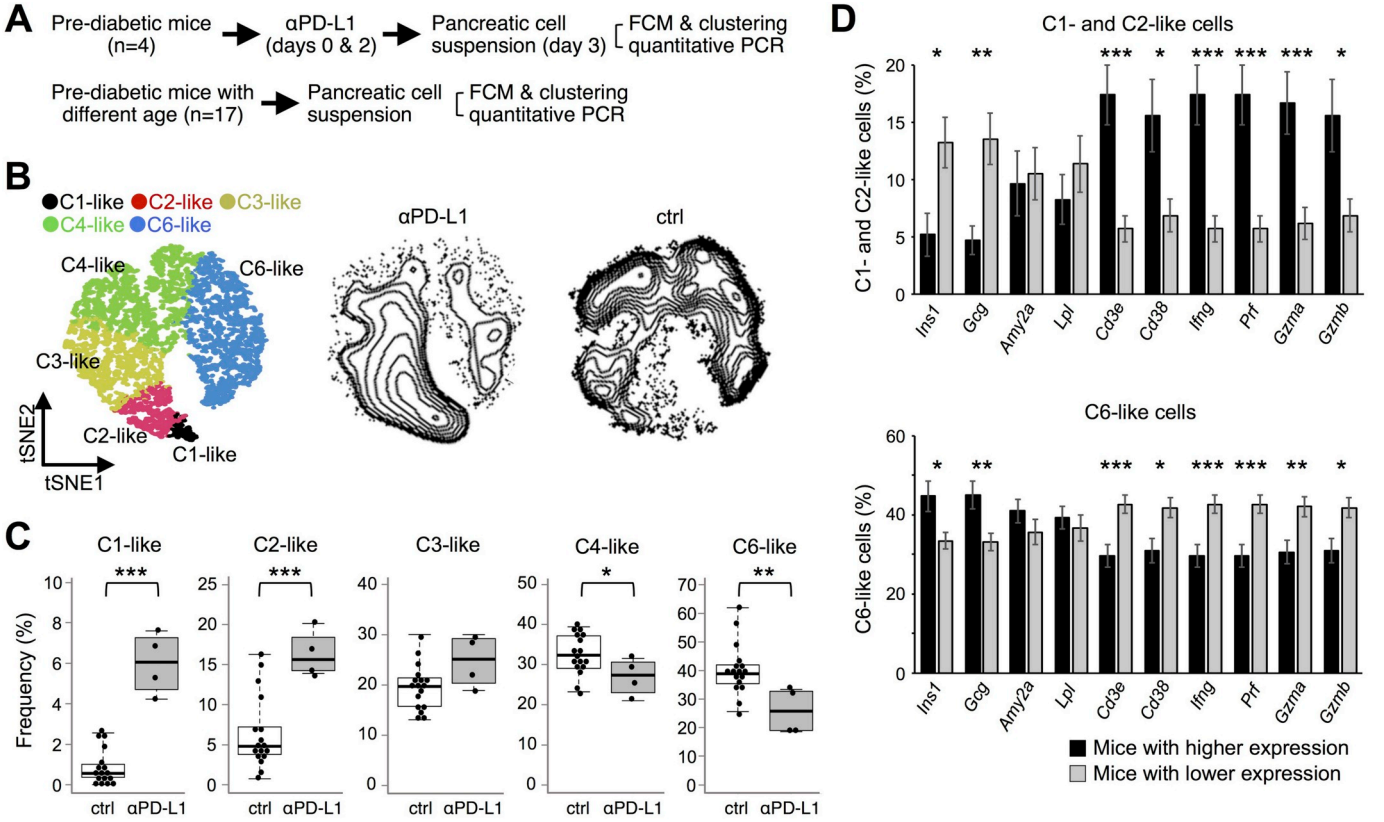

Fig. 5. Correlation between cluster composition and disease status of T1D in NOD mice. (A) Schematic representation of the sample preparation. Pancreatic cell suspension was divided into two for flowcytometry (FCM) and quantitative PCR. (B) Classification of PD-1$^+$CD8$^+$ T cells into C1-, C2-, C3-, C4-, and C6-like clusters. A *t*-SNE plot of islet-infiltrating PD-1$^+$CD8$^+$ T cells overlaid with the color-coded clusters (left). Density *t*-SNE plots of islet-infiltrating PD-1$^+$CD8$^+$ T cells from NOD mice treated with (middle, n = 4) or without (right, n = 17) αPD-L1. (C) Increase of C1- and C2-like cells and decrease of C4- and C6-like cells by PD-1 blockade. (D) Correlation between cluster composition and disease status. Frequencies of C1- and C2-like (top) and C6-like (bottom) cells are shown for mice with higher (black) and lower (gray) expression of indicated genes. Two-tailed paired Student's *t*-test (C and D). $^*P < 0.05$, $^{**}P < 0.01$, $^{***}P < 0.005$. (For interpretation of the references to color in this figure legend, the reader is referred to the Web version of this article.)

We also hypothesized that the cluster composition of tumor-specific T cells before *anti*-PD-1 therapy influence the efficacy of the therapy. We picked up genes that represent the signature of cells with active suppression by PD-1 (i.e., genes highly expressed in C3–4 compared with C6 cells) and examined their expression in tumor-tissues before *anti*-PD-1 therapy. Intriguingly, genes representing the relative increase of C3–4 over C6 showed higher expression in melanoma tissues of responders compared with those of non-responders before *anti*-PD-1 therapy (Fig. 6D–F). These results indicate that *anti*-PD-1 therapy is more efficacious when tumor-infiltrating cells are actively suppressed by PD-1 (i.e., at C3–4) but are not functionally impaired (i.e., at C6) before the start of *anti*-PD-1 therapy. Thus, the cluster composition of T cells and the expression of genes representing the activation trajectory of CD8$^+$ T cells in tumor tissues can be useful prognostic-markers for *anti*-PD-1 therapy.

4. Discussion

In the current study, we delineated the activation trajectory of autoreactive CD8$^+$ T cells in T1D by comparing autoreactive CD8$^+$ T cells under or beyond the control of PD-1. Autoreactive CD8$^+$ T cells went through four activation-phases and PD-1 strongly attenuated the transition from the second- to the third-phase, where autoreactive CD8$^+$ T cells acquired effector function. We detected the up-regulation of *Foxo1* in C3 cells where the stepwise activation was suspended by PD-1. Because FoxO1 has been reported to hinder the effector differentiation of CD8$^+$ T cells by up-regulating *Pdcd1* [41,42], FoxO1–PD-1 axis may partly explain the interruption of the activation trajectory at C3 in the PD-1-sufficient condition. The majority of autoreactive CD8$^+$ T cells under the control of PD-1 showed an intensively inactivated signature and exhibited a distinct trajectory in pseudotemporal ordering.

The shifts in cluster composition markedly reflected the damage of target tissues and the severity of inflammation in T1D of NOD mice. In addition, genes that were up-regulated along with the activation trajectory in T1D showed higher expression in melanoma tissues of responders compared with those of non-responders in *anti*-PD-1 therapy, indicating that tumor specific T cells can destroy tumor-tissues efficiently in human melanoma patients upon *anti*-PD-1 therapy when they are successfully activated in a similar trajectory found in T1D. Besides, genes representing cells with the active but not intensive suppression by PD-1 showed higher expression in melanoma tissues of responders compared with those of non-responders before the start of *anti*-PD-1 therapy, which is in agreement with the higher abundance of partially exhausted tumor-infiltrating CD8$^+$ T cells in responders of *anti*-PD-1 therapy in the former study [19]. Thus, the fine clustering of tumor-specific T cells before *anti*-PD-1 therapy can be a useful strategy to predict the efficacy of *anti*-PD-1 therapy. Because of the limited response rates of *anti*-PD-1 therapy, markers to distinguish responders from non-responders are extensively explored [18–21,48,49]. By delineating the activation trajectory of CD8$^+$ T cells upon PD-1 blockade, we could identify genes that accurately signify the activation status of CD8$^+$ T cells and demonstrate their potencies as predictive markers.

Today, the role of PD-1 as a suppressor of T cells is widely accepted and *anti*-PD-1 therapy is used worldwide. However, how CD8$^+$ T cells are activated to eradicate tumor cells or damage self-tissues upon *anti*-PD-1 therapy remain unclear. Actually, the increase of exhausted rather

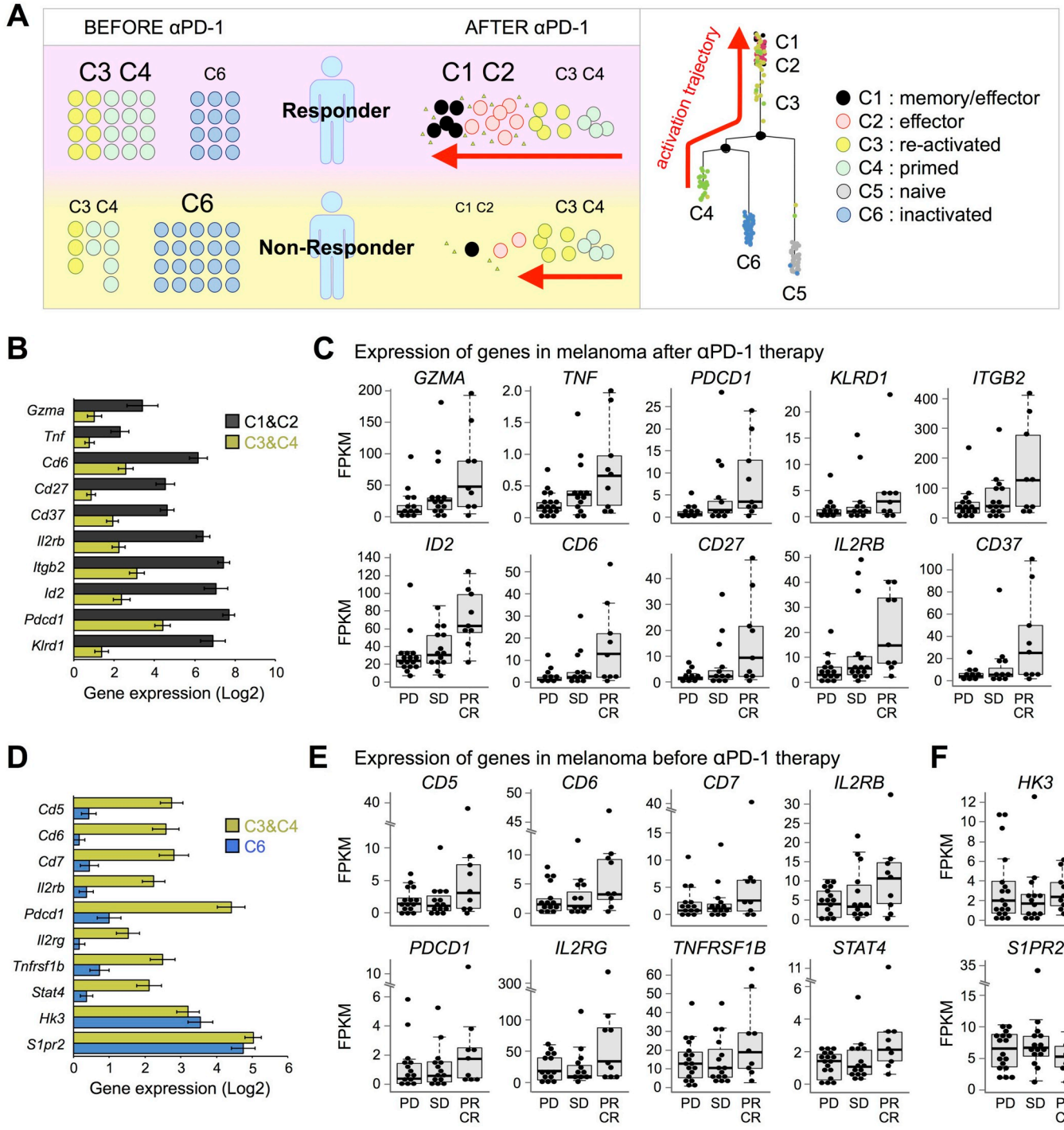

Fig. 6. Tumor-specific T cells are activated in a similar trajectory found in T1D to destroy tumor-tissues in human melanoma patients upon *anti*-PD-1 therapy. (A) Schematic representation of the two hypotheses. *Anti*-PD-1 therapy is expected to be more efficacious when tumor-infiltrating T cells are actively suppressed by PD-1 (i.e., at C3–4) but are not functionally impaired (i.e., at C6) before *anti*-PD-1 therapy (left). *Anti*-PD-1 therapy is expected to enable tumor specific T cells in a similar activation trajectory found in T1D in responders of *anti*-PD-1 therapy (middle). The activation trajectory of autoreactive $CD8^+$ T cell upon *anti*-PD-1 therapy in NOD mice is shown in the right side. (B and C) Genes representing the progression of the activation trajectory in T1D showed higher expression in melanoma-tissues of responders upon *anti*-PD-1 therapy. Bar graphs showing the expression levels of indicated genes in C1–2 and C3–4 cells (B). Box plots showing the expression levels (FPKMs) of indicated genes in melanoma-tissues upon *anti*-PD-1 therapy (C). (D–F) Genes representing the dominance of C3–4 over C6 in T1D showed higher expression in melanoma-tissues of responders before *anti*-PD-1 therapy. Bar graphs showing the expression levels of indicated genes in C3–4 and C6 cells (D). Box plots showing the expression levels of indicated genes in melanoma-tissues before *anti*-PD-1 therapy. Genes with higher (E) or comparable (F) expression levels in C3–4 cells compared with C6 cells are shown. PD, progressive disease (n = 18); SD, stable disease (n = 15); PR, partial response (n = 6); CR, complete response (n = 3) (C, E, and F).

than activated $CD8^+$ T cells in tumor tissues have been observed as hallmarks of PD-1 blockade at single cell level, which is rather paradoxical to its curative effect. Wei et al. reported that $CD8^+$ T cells with Tex-like features were increased by *anti*-PD-1 therapy in tumors of mice and human patients using mass-cytometry [23]. Gubin et al. also reported the increase of cells with the lowest Granzyme B expression

upon PD-1 blockade in mice using mass-cytometry [24]. On the other hand, Sade-Feldman et al. identified memory/effector-like clusters of $CD8^+$ T cells whose frequencies were higher in melanoma tissues of responders compared with non-responders in *anti*-PD-1 therapy using single cell RNA sequencing [25]. However, they reported that there was no significant change between before and after *anti*-PD-1 therapy, indicating that the differences were likely related to features of tumors and/or microenvironments rather than PD-1 blockade itself. Although single cell RNA sequencing is a very powerful method, the sensitivity for the detection of low-expressing genes is rather low, which may limit the fine characterization of cells. Thus, the activation of $CD8^+$ T cells upon *anti*-PD-1 blockade has not been evident in former single cell analyses contrary to the general expectations, making the cellular mechanisms of tumor-eradication and irAEs by *anti*-PD-1 therapy remain to be clarified.

Compared with mass-cytometry and single cell RNA sequencing, the current method has a limitation in the number of analyzable cells but has a better sensitivity for the detection of genes with relatively low expression [50]. In pre-diabetic NOD mice, autoreactive $CD8^+$ T cells were readily activated and destroyed pancreateatic β cells upon PD-1 blockade. Because a substantial proportion but not all of islet-infiltrating $CD8^+$ T cells proliferated upon PD-1 blockade, islet-infiltrating $CD8^+$ T cells were likely composed of cells at diverse stages of the activation and cell cycle. We took the advantage of this rapid induction of T1D and analyzed autoreactive $CD8^+$ T cells just before they completely eradicate β cells. Remarkably, we could detect autoreactive $CD8^+$ T cells with four different activation phases among no more than 175 cells, indicating that the activation of autoreactive $CD8^+$ T cells is a rapid and dynamic process. These results highlight the importance of pinpointing $CD8^+$ T cells that are being activated and quantifying functionally relevant genes for the elucidation of the actual activation status of $CD8^+$ T cells especially in *anti*-PD-1 therapy.

Our current findings revealed the activation trajectory of autoreactive $CD8^+$ T cells in the target tissue and clearly demonstrated the rapid and massive increase of activated T cells by PD-1 blockade, which parallels with disease progression. Precise and deeper understandings of PD-1 effects on the activation trajectory of T cells are expected to elucidate the pathomechanisms of spontaneous as well as *anti*-PD-1 related autoimmune diseases and facilitate the rational design of immunotherapies.

Author contributions

HO, IO, and TO designed the experiments. HO, IO, TM, DS, RM, and KS established experimental systems and performed experiments. HO, IO, and KS analyzed the data. HO, IO, and TO wrote the manuscript with all authors contributing to writing. TO supervised the project.

Conflicts of interest

The authors declare no competing financial interests.

Acknowledgments

We thank M. Ono for helpful discussion; Y. Okamoto, M. Aoki, H. Tsuduki, and R. Matsumura for technical and secretarial assistances; other members of our laboratory for helpful discussions. This work was supported in part by the Japan Science and Technology Agency (TO), Grant-in-Aid by the Japan Society for the Promotion of Science (JP18H05417, TO; JP19H01029, TO; JP15K9132, IO), and Uehara Memorial Foundation (TO).

Appendix A. Supplementary data

Supplementary data to this article can be found online at https://doi.org/10.1016/j.jaut.2019.06.007.

References

[1] J.R. Brahmer, C.G. Drake, I. Wollner, J.D. Powderly, J. Picus, W.H. Sharfman, et al., Phase I study of single-agent anti-programmed death-1 (MDX-1106) in refractory solid tumors: safety, clinical activity, pharmacodynamics, and immunologic correlates, J. Clin. Oncol. 28 (2010) 3167–3175.
[2] Y. Iwai, M. Ishida, Y. Tanaka, T. Okazaki, T. Honjo, N. Minato, Involvement of PD-L1 on tumor cells in the escape from host immune system and tumor immunotherapy by PD-L1 blockade, Proc. Natl. Acad. Sci. U. S. A. 99 (2002) 12293–12297.
[3] T. Okazaki, S. Chikuma, Y. Iwai, S. Fagarasan, T. Honjo, A rheostat for immune responses: the unique properties of PD-1 and their advantages for clinical application, Nat. Immunol. 14 (2013) 1212–1218.
[4] A. Ribas, J.D. Wolchok, Cancer immunotherapy using checkpoint blockade, Science 359 (2018) 1350–1355.
[5] F.A. Schildberg, S.R. Klein, G.J. Freeman, A.H. Sharpe, Coinhibitory pathways in the B7-CD28 ligand-receptor family, Immunity 44 (2016) 955–972.
[6] C. Sun, R. Mezzadra, T.N. Schumacher, Regulation and function of the PD-L1 checkpoint, Immunity 48 (2018) 434–452.
[7] J.M. Chemnitz, R.V. Parry, K.E. Nichols, C.H. June, J.L. Riley, SHP-1 and SHP-2 associate with immunoreceptor tyrosine-based switch motif of programmed death 1 upon primary human T cell stimulation, but only receptor ligation prevents T cell activation, J. Immunol. 173 (2004) 945–954.
[8] E. Hui, J. Cheung, J. Zhu, X. Su, M.J. Taylor, H.A. Wallweber, et al., T cell costimulatory receptor CD28 is a primary target for PD-1-mediated inhibition, Science 355 (2017) 1428–1433.
[9] H. Nishimura, T. Okazaki, Y. Tanaka, K. Nakatani, M. Hara, A. Matsumori, et al., Autoimmune dilated cardiomyopathy in PD-1 receptor-deficient mice, Science 291 (2001) 319–322.
[10] T. Yokosuka, M. Takamatsu, W. Kobayashi-Imanishi, A. Hashimoto-Tane, M. Azuma, T. Saito, Programmed cell death 1 forms negative costimulatory microclusters that directly inhibit T cell receptor signaling by recruiting phosphatase SHP2, J. Exp. Med. 209 (2012) 1201–1217.
[11] R. Mizuno, D. Sugiura, K. Shimizu, T. Maruhashi, M. Watada, I.M. Okazaki, et al., PD-1 primarily targets TCR signal in the inhibition of functional T cell activation, Front. Immunol. 10 (2019) 630.
[12] S. Chikuma, S. Terawaki, T. Hayashi, R. Nabeshima, T. Yoshida, S. Shibayama, et al., PD-1-mediated suppression of IL-2 production induces CD8 + T cell anergy in vivo, J. Immunol. 182 (2009) 6682–6689.
[13] L.M. Francisco, V.H. Salinas, K.E. Brown, V.K. Vanguri, G.J. Freeman, V.K. Kuchroo, et al., PD-L1 regulates the development, maintenance, and function of induced regulatory T cells, J. Exp. Med. 206 (2009) 3015–3029.
[14] D.L. Barber, E.J. Wherry, D. Masopust, B. Zhu, J.P. Allison, A.H. Sharpe, et al., Restoring function in exhausted CD8 T cells during chronic viral infection, Nature 439 (2006) 682–687.
[15] S.D. Blackburn, H. Shin, W.N. Haining, T. Zou, C.J. Workman, A. Polley, et al., Coregulation of CD8 + T cell exhaustion by multiple inhibitory receptors during chronic viral infection, Nat. Immunol. 10 (2009) 29–37.
[16] C.L. Day, D.E. Kaufmann, P. Kiepiela, J.A. Brown, E.S. Moodley, S. Reddy, et al., PD-1 expression on HIV-specific T cells is associated with T-cell exhaustion and disease progression, Nature 443 (2006) 350–354.
[17] K.E. Pauken, M.A. Sammons, P.M. Odorizzi, S. Manne, J. Godec, O. Khan, et al., Epigenetic stability of exhausted T cells limits durability of reinvigoration by PD-1 blockade, Science 354 (2016) 1160–1165.
[18] M. Ayers, J. Lunceford, M. Nebozhyn, E. Murphy, A. Loboda, D.R. Kaufman, et al., IFN-gamma-related mRNA profile predicts clinical response to PD-1 blockade, J. Clin. Investig. 127 (2017) 2930–2940.
[19] A.I. Daud, K. Loo, M.L. Pauli, R. Sanchez-Rodriguez, P.M. Sandoval, K. Taravati, et al., Tumor immune profiling predicts response to anti-PD-1 therapy in human melanoma, J. Clin. Investig. 126 (2016) 3447–3452.
[20] A. Prat, A. Navarro, L. Pare, N. Reguart, P. Galvan, T. Pascual, et al., Immune-related gene expression profiling after PD-1 blockade in non-small cell lung carcinoma, head and neck squamous cell carcinoma, and melanoma, Cancer Res. 77 (2017) 3540–3550.
[21] N. Riaz, J.J. Havel, V. Makarov, A. Desrichard, W.J. Urba, J.S. Sims, et al., Tumor and microenvironment evolution during immunotherapy with Nivolumab, Cell 171 (2017) 934-49 e16.
[22] A.C. Huang, M.A. Postow, R.J. Orlowski, R. Mick, B. Bengsch, S. Manne, et al., T-cell invigoration to tumour burden ratio associated with anti-PD-1 response, Nature 545 (2017) 60–65.
[23] S.C. Wei, J.H. Levine, A.P. Cogdill, Y. Zhao, N.A.S. Anang, M.C. Andrews, et al., Distinct cellular mechanisms underlie anti-CTLA-4 and anti-PD-1 checkpoint blockade, Cell 170 (2017) 1120–1133 e17.
[24] M.M. Gubin, E. Esaulova, J.P. Ward, O.N. Malkova, D. Runci, P. Wong, et al., High-dimensional analysis delineates myeloid and lymphoid compartment remodeling during successful immune-checkpoint cancer therapy, Cell 175 (2018) 1014–1030 e19.
[25] M. Sade-Feldman, K. Yizhak, S.L. Bjorgaard, J.P. Ray, C.G. de Boer, R.W. Jenkins, et al., Defining T cell states associated with response to checkpoint immunotherapy in melanoma, Cell 175 (2018) 998–1013 e20.
[26] M. Ishida, Y. Iwai, Y. Tanaka, T. Okazaki, G.J. Freeman, N. Minato, et al., Differential expression of PD-L1 and PD-L2, ligands for an inhibitory receptor PD-1, in the cells of lymphohematopoietic tissues, Immunol. Lett. 84 (2002) 57–62.
[27] T. Maruhashi, I.M. Okazaki, D. Sugiura, S. Takahashi, T.K. Maeda, K. Shimizu, et al., LAG-3 inhibits the activation of CD4(+) T cells that recognize stable pMHCII

through its conformation-dependent recognition of pMHCII, Nat. Immunol. 19 (2018) 1415–1426.
[28] M.J. Ansari, A.D. Salama, T. Chitnis, R.N. Smith, H. Yagita, H. Akiba, et al., The programmed death-1 (PD-1) pathway regulates autoimmune diabetes in nonobese diabetic (NOD) mice, J. Exp. Med. 198 (2003) 63–69.
[29] K.C. Herold, D.A. Vignali, A. Cooke, J.A. Bluestone, Type 1 diabetes: translating mechanistic observations into effective clinical outcomes, Nat. Rev. Immunol. 13 (2013) 243–256.
[30] J. Wang, T. Yoshida, F. Nakaki, H. Hiai, T. Okazaki, T. Honjo, Establishment of NOD-Pdcd1-/- mice as an efficient animal model of type I diabetes, Proc. Natl. Acad. Sci. U. S. A. 102 (2005) 11823–11828.
[31] M.E. Keir, S.C. Liang, I. Guleria, Y.E. Latchman, A. Qipo, L.A. Albacker, et al., Tissue expression of PD-L1 mediates peripheral T cell tolerance, J. Exp. Med. 203 (2006) 883–895.
[32] D. Sugiura, T. Maruhashi, I.M. Okazaki, K. Shimizu, T.K. Maeda, T. Takemoto, et al., Restriction of PD-1 function by cis-PD-L1/CD80 interactions is required for optimal T cell responses, Science 364 (2019) 558–566.
[33] E.J. Wherry, M. Kurachi, Molecular and cellular insights into T cell exhaustion, Nat. Rev. Immunol. 15 (2015) 486–499.
[34] Y. Agata, A. Kawasaki, H. Nishimura, Y. Ishida, T. Tsubata, H. Yagita, et al., Expression of the PD-1 antigen on the surface of stimulated mouse T and B lymphocytes, Int. Immunol. 8 (1996) 765–772.
[35] X. Qiu, Q. Mao, Y. Tang, L. Wang, R. Chawla, H.A. Pliner, et al., Reversed graph embedding resolves complex single-cell trajectories, Nat. Methods 14 (2017) 979–982.
[36] B.T. Endrizzi, S.C. Jameson, Differential role for IL-7 in inducing lung Kruppel-like factor (Kruppel-like factor 2) expression by naive versus activated T cells, Int. Immunol. 15 (2003) 1341–1348.
[37] C.T. Kuo, M.L. Veselits, J.M. Leiden, LKLF: a transcriptional regulator of single-positive T cell quiescence and survival, Science 277 (1997) 1986–1990.
[38] A.J. Menner, K.S. Rauch, P. Aichele, H. Pircher, C. Schachtrup, K. Schachtrup, Id3 controls cell death of 2B4+ virus-specific CD8+ T cells in chronic viral infection, J. Immunol. 195 (2015) 2103–2114.
[39] T. Willinger, T. Freeman, M. Herbert, H. Hasegawa, A.J. McMichael, M.F. Callan, Human naive CD8 T cells down-regulate expression of the WNT pathway transcription factors lymphoid enhancer binding factor 1 and transcription factor 7 (T cell factor-1) following antigen encounter in vitro and in vivo, J. Immunol. 176 (2006) 1439–1446.
[40] C.Y. Yang, J.A. Best, J. Knell, E. Yang, A.D. Sheridan, A.K. Jesionek, et al., The transcriptional regulators Id2 and Id3 control the formation of distinct memory CD8+ T cell subsets, Nat. Immunol. 12 (2011) 1221–1229.
[41] R. Hess Michelini, A.L. Doedens, A.W. Goldrath, S.M. Hedrick, Differentiation of CD8 memory T cells depends on Foxo1, J. Exp. Med. 210 (2013) 1189–1200.
[42] M.M. Staron, S.M. Gray, H.D. Marshall, I.A. Parish, J.H. Chen, C.J. Perry, et al., The transcription factor FoxO1 sustains expression of the inhibitory receptor PD-1 and survival of antiviral CD8(+) T cells during chronic infection, Immunity 41 (2014) 802–814.
[43] M.D. Buck, D. O'Sullivan, E.L. Pearce, T cell metabolism drives immunity, J. Exp. Med. 212 (2015) 1345–1360.
[44] S.M. Kaech, W. Cui, Transcriptional control of effector and memory CD8+ T cell differentiation, Nat. Rev. Immunol. 12 (2012) 749–761.
[45] G. Xin, D.M. Schauder, B. Lainez, J.S. Weinstein, Z. Dai, Y. Chen, et al., A critical role of IL-21-induced BATF in sustaining CD8-T-cell-mediated chronic viral control, Cell Rep. 13 (2015) 1118–1124.
[46] J. Crespo, H. Sun, T.H. Welling, Z. Tian, W. Zou, T cell anergy, exhaustion, senescence, and stemness in the tumor microenvironment, Curr. Opin. Immunol. 25 (2013) 214–221.
[47] E.J. Wherry, S.J. Ha, S.M. Kaech, W.N. Haining, S. Sarkar, V. Kalia, et al., Molecular signature of CD8+ T cell exhaustion during chronic viral infection, Immunity 27 (2007) 670–684.
[48] N.A. Rizvi, M.D. Hellmann, A. Snyder, P. Kvistborg, V. Makarov, J.J. Havel, et al., Cancer immunology. Mutational landscape determines sensitivity to PD-1 blockade in non-small cell lung cancer, Science 348 (2015) 124–128.
[49] P.C. Tumeh, C.L. Harview, J.H. Yearley, I.P. Shintaku, E.J. Taylor, L. Robert, et al., PD-1 blockade induces responses by inhibiting adaptive immune resistance, Nature 515 (2014) 568–571.
[50] T. Kroneis, E. Jonasson, D. Andersson, S. Dolatabadi, A. Stahlberg, Global pre-amplification simplifies targeted mRNA quantification, Sci. Rep. 7 (2017) 45219.